THE JOURNAL OF BIOLOGICAL CHEMISTRY VOL. 285, NO. 4, pp. 2245–2257, January 22, 2010
© 2010 by The American Society for Biochemistry and Molecular Biology, Inc. Printed in the U.S.A.

Cluster Analysis of Insulin Action in Adipocytes Reveals a Key Role for Akt at the Plasma Membrane*[S]

Received for publication, August 27, 2009, and in revised form, October 19, 2009 Published, JBC Papers in Press, November 6, 2009, DOI 10.1074/jbc.M109.060236

Yvonne Ng[‡§], Georg Ramm[‡¶], James G. Burchfield[‡], Adelle C. F. Coster[‡‖], Jacqueline Stöckli[‡1], and David E. James[‡§2]**

*From the [‡]Diabetes and Obesity Research Program, The Garvan Institute of Medical Research, Sydney, New South Wales 2010, the [§]School of Biotechnology and Biomolecular Sciences, [‖]School of Mathematics and Statistics, and **Faculty of Medicine, University of New South Wales, Sydney, New South Wales 2052, and the [¶]School of Biomedical Sciences, Monash University, Melbourne, Victoria 3800, Australia*

The phosphatidylinositol 3-kinase/Akt pathway regulates many biological processes, including insulin-regulated GLUT4 insertion into the plasma membrane. However, Akt operates well below its capacity to facilitate maximal GLUT4 translocation. Thus, reconciling modest changes in Akt expression or activity as a cause of metabolic dysfunction is complex. To resolve this, we examined insulin regulation of components within the signaling cascade in a quantitative kinetic and dose-response study combined with hierarchical cluster analysis. This revealed a strong relationship between phosphorylation of Akt substrates and GLUT4 translocation but not whole cell Akt phosphorylation. In contrast, Akt activity at the plasma membrane strongly correlated with GLUT4 translocation and Akt substrate phosphorylation. Additionally, two of the phosphorylated sites in the Akt substrate AS160 clustered separately, with Thr(P)-642 grouped with other Akt substrates. Further experiments suggested that atypical protein kinase Cζ phosphorylates AS160 at Ser-588 and that these two sites are mutually exclusive. These data indicate the utility of hierarchical cluster analysis for identifying functionally related biological nodes and highlight the importance of subcellular partitioning of key signaling components for biological specificity.

The receptor tyrosine kinase family is both large and diverse controlling a broad spectrum of fundamental biological processes, including cell death, differentiation, and proliferation. Curiously, these diverse processes are controlled by a limited subset of canonical signaling modules typified by the phosphatidylinositol 3-kinase (PI[3] 3-kinase)/Akt and Ras/MAPK pathways. But how do relatively few signaling pathways control such a diversity of actions? To answer this question, it is essential to identify pathway components and to understand how they interact in different cells under a range of conditions. Considerable information about the components that include the PI 3-kinase/Akt pathway is known (1). Activation of a receptor tyrosine kinase at the plasma membrane (PM) generates a binding site for the p85 regulatory subunit of PI 3-kinase allowing for production of phosphatidylinositol 3,4,5-trisphosphate at the PM. Phosphatidylinositol 3,4,5-trisphosphate serves as a docking site for proteins such as PDK1 (phosphoinositide-dependent kinase 1) and Akt that possess lipid-binding domains. This presumably concentrates Akt with its upstream regulatory kinases PDK1 and mammalian target of rapamycin-rictor complex (2, 3) resulting in Akt phosphorylation at Thr-308 and Ser-473, respectively. Phosphorylation at these sites leads to a regulatory conformational change in Akt that facilitates its interaction with downstream substrates. Numerous Akt substrates possessing the Akt kinase consensus motif R*X*R*XX*(S/T) have been identified, and these have been implicated in a range of fundamental biological processes (4).

Evidence points to a major role for Akt in almost all of the metabolic actions of insulin (5). This includes the regulation of glucose transport that is mediated via the regulated translocation of the GLUT4 (glucose transporter 4) to the PM, glycogen synthesis, protein synthesis, lipolysis, and transcription. In each of these cases, Akt substrates that control these processes have been identified as follows: the RabGAP AS160/TBC1D4 (6); GSK3 (glycogen synthase kinase 3) (7); the RhebGAP TSC2 (tuberous sclerosis protein 2) (8); PDE3B (phosphodiesterase 3B) (9), and FoxO (10). Although many of these molecules are ubiquitous and many growth factors control the PI 3-kinase/Akt pathway, there are several facets of the insulin pathway that are unique as follows: insulin regulation of metabolism is confined to muscle, adipose tissue, and liver (5); the insulin pathway utilizes the insulin receptor substrate (IRS) scaffold protein family to orchestrate upstream activation of the Akt pathway (11); and metabolism is thought to be controlled by certain signaling isoforms within the PI 3-kinase/Akt pathway, including the p110α PI 3-kinase catalytic subunit (12, 13) and the Akt2 isoform (14–16).

Impaired insulin action or insulin resistance plays a central role in a range of metabolic diseases, including type 2 diabetes. Here, it is generally considered that a defect in one or more of the upstream components of the PI 3-kinase/Akt pathway results in attenuation of signal transmission through Akt lead-

* This work was supported in part by grants from the National Health and Medical Research Council of Australia.

[S] The on-line version of this article (available at http://www.jbc.org) contains supplemental Fig. 1 and Table I.

[1] Supported by fellowships from the Swiss National Foundation and Novartis Foundation.

[2] National Health and Medical Research Council Senior Principal Research Fellow. To whom correspondence should be addressed. Tel.: 61-2-92958210; Fax: 61-2-92958201; E-mail: d.james@garvan.org.au.

[3] The abbreviations used are: PI, phosphatidylinositol; PM, plasma membrane; IRS, insulin receptor substrate; PDGF, platelet-derived growth factor; PDGFR, PDGF receptor; DMEM, Dulbecco's modified Eagle's medium; BSA, bovine serum albumin; PBS, phosphate-buffered saline; MES, 4-morpholineethanesulfonic acid; PKC, protein kinase C; MAPK, mitogen-activated protein kinase; TCL, total cell lysate; LDM, low density microsome; TIRF, total internal refection fluorescence.

ing to global dysregulation of insulin action. For example, a modest reduction in tyrosine phosphorylation of IRS1 will lead to a modest reduction in PI 3-kinase activation in turn leading to a modest reduction in Akt activation and so on. This implies the existence of a robust coupling mechanism between each of the components that define the system. One prediction from this is that each of the components that include a functionally related node will exhibit behavioral kinship that should be measurable. However, we have recently observed features of the Akt node that do not support this hypothesis. Biological outputs such as GLUT4 translocation achieve a maximal stimulatory level at insulin concentrations that are sufficient to activate as little as 10–20% of the total cellular Akt pool (17, 18). Thus, this implies that Akt operates well below its maximal capacity. Under physiological conditions, most processes have evolved to operate over the steepest and most responsive part of their intrinsic range. However, this appears not to be the case for Akt. Intuitively, it is difficult to envisage how minute changes in Akt activity could accurately translate into large biological changes of the kind observed for GLUT4 translocation and so on. Consistent with this anomalous behavior, we recently observed that in a range of insulin resistance models where defects in Akt activity were in some cases evident, there was little parity between this and phosphorylation of other substrates such as the AS160 or GLUT4 translocation (17). In this study, we set out to investigate the topology of a range of components within the insulin-signaling network to test the behavioral kinship hypothesis. We found that a simple dose-response analysis provided a powerful behavioral index of individual components. Hierarchical cluster analysis allowed us to sort components into related groups providing the first clue that Akt phosphorylation at either Thr-308 or Ser-473 in whole cells maintains a poor relationship with insulin-dependent phosphorylation of a range of Akt substrates, including AS160, GSK3, FoxO, and TSC2. In contrast, there was a strong relationship between Akt phosphorylation at the PM with GLUT4 translocation and AS160 phosphorylation at its major 14-3-3-binding site Thr-642. Interestingly, among the Akt substrates, AS160 is clustered closest to GLUT4 translocation. This is striking because AS160, but none of the other substrates, has been implicated as a major regulator of GLUT4 translocation. Hence, these studies support a model of behavioral kinship suggesting that similar analyses might be useful in mapping functional signaling nodes within complex networks. Our studies also show that subcellular localization of signaling components is likely one of the major determinants of specificity, and so in terms of mapping mechanistic disease loci this may represent a major target.

EXPERIMENTAL PROCEDURES

Materials—Polyclonal rabbit antibodies raised against total Akt, Thr(P)-308 Akt, total GSK3β, Ser(P)-21/9 GSK-3α/β, Thr(P)-389 S6 kinase, Ser(P)-256 FoxO1, Thr(P)-1462 TSC2, and monoclonal rabbit antibodies raised against Ser(P)-473 Akt (193H12) (for immunofluorescence), glyceraldehyde-3-phosphate dehydrogenase, phospho-Akt substrate, and phospho-(Ser) PKC substrate, and mouse monoclonal antibody raised against Ser(P)-473 Akt (for Western blot) and Thr(P)-202/Tyr(P)-204 MAPK were purchased from Cell Signaling Technologies (Beverly, MA). Polyclonal rabbit antibodies raised against TSC2, FoxO1, and 14-3-3β were purchased from Santa Cruz Biotechnology, Inc. (Santa Cruz, CA). Polyclonal AS160 antibody was from Upstate Biotechnology, Inc. (Lake Placid, NY), and monoclonal hemagglutinin antibody was from Covance (Berkeley, CA). The mouse monoclonal antibodies raised against Crk and caveolin were from BD Transduction Laboratories. The mouse FLAG (M2) antibody was from Sigma, and mouse monoclonal V5 antibody was from Invitrogen. The affinity-purified rabbit polyclonal Thr(P)-642 AS160 raised against the mouse Thr(P)-649 AS160 from amino acids 642–655 (QFRRRAHpTFSHPPS) was custom-made by 21st Century Biochemicals (Marlboro, MA). Antibodies against mouse monoclonal GLUT4 and rabbit polyclonal insulin-responsive aminopeptidase were described previously (19). Horseradish peroxidase-conjugated secondary antibodies were from Amersham Biosciences; IR dye 700- or 800-conjugated secondary antibodies were from Rockland Immunochemicals (Gilbertsville, PA); Alexa488-conjugated secondary antibody was from Molecular Probes (Leiden, The Netherlands); and Cy2-conjugated secondary antibody was obtained from Jackson ImmunoResearch (West Grove, PA). Polyclonal sheep antibodies raised against Ser(P)-588 AS160 and Thr(P)-642 AS160 and the Akt-i1/2 specific inhibitor were obtained from Peter Shepherd (Symansis, Auckland, New Zealand). Paraformaldehyde was from ProSciTech (Thuringowa, Australia). Insulin was purchased from Calbiochem; Dulbecco's modified Eagle's medium (DMEM), newborn calf serum, and Lipofectamine 2000 were from Invitrogen; fetal calf serum was from Trace Scientific (Melbourne, Australia); and antibiotics were from Invitrogen. Bovine serum albumin (BSA) was from Bovogen (Essendon, Australia); BCA reagent was from SuperSignal West Pico; and chemiluminescent substrate and protein G-Sepharose beads were from Pierce. Complete protease inhibitor mixture tablets were from Roche Applied Science. FLAG AS160 mutant plasmids were described previously (20). All other materials were obtained from Sigma.

Cell Culture and Transfections—3T3-L1 fibroblasts (ATCC, Manassas, VA) were cultured and differentiated into adipocytes as described previously (21). 3T3-L1 fibroblasts were infected with pBabepuro-HA-GLUT4 retrovirus or pLXSN PDGFR wild-type retrovirus. After 24 h, infected cells were selected with either 2 μg/ml puromycin or 800 μg/ml geneticin in DMEM supplemented with 10% fetal calf serum for selection of HA-GLUT4-infected cells or PDGFR-infected cells, respectively. Surviving cells were split and differentiated as described above. HEK 293 cells (Invitrogen) were cultured in DMEM supplemented with 10% fetal calf serum. Cells were transfected with respective constructs using Lipofectamine 2000 according to the manufacturer's protocol.

Western Blotting Analysis—3T3-L1 adipocytes were incubated in DMEM with 0.2% BSA for 2 h before stimulation with the indicated time and dose of insulin or PDGF. Cells were then washed twice with ice-cold phosphate-buffered saline (PBS) and harvested in PBS with 1% SDS supplemented with Complete protease inhibitor mixture and phosphatase inhibitors (2 mM sodium orthovanadate, 1 mM pyrophosphate, 10 mM

sodium fluoride). Insoluble material was removed by centrifugation at 18,000 × *g* for 20 min at 24 °C. Protein concentration was measured using the BCA protein assay, and proteins were separated by SDS-PAGE for immunoblot analysis. After transferring proteins to polyvinylidene difluoride membranes, membranes were incubated in blocking buffer containing 5% skim milk in Tris-buffered saline and immunoblotted with respective antibodies overnight at 4 °C in blocking buffer containing 5% BSA, 0.1% Tween in Tris-buffered saline. After incubation, membranes were washed and incubated with horseradish peroxidase-labeled secondary antibodies, and then detected by Supersignal West Pico chemiluminescent substrate. In some cases, IR dye 700- or 800-conjugated secondary antibodies were used. Membranes were then scanned in the 700 or 800 nM channel using the Odyssey IR imager. Quantification of protein levels was performed using Odyssey IR imaging system software or the Wright Cell Imaging Facility ImageJ software.

Immunoprecipitation—Following stimulations, cells were washed with ice-cold PBS and solubilized in RIPA buffer (50 mM Tris-HCl, pH 7.5, 150 mM NaCl, 1% Triton X-100, 0.5% sodium deoxycholate, 0.1% SDS, 1 mM EDTA, and 10% glycerol) containing Complete protease inhibitor mixture and phosphatase inhibitors (2 mM sodium orthovanadate, 1 mM sodium pyrophosphate, 10 mM sodium fluoride). Cell lysates were homogenized 10 times using a 27-gauge needle and centrifuged at 18,000 × *g* for 20 min at 4 °C. Two mg of cell lysates were incubated overnight at 4 °C with 4 μg of polyclonal rabbit Thr(P)-642 AS160 or nonimmunized rabbit IgG. Antibodies were then captured with protein G-Sepharose beads for 2 h at 4 °C. Immunoprecipitates were washed extensively with ice-cold RIPA buffer and kept in 2× SDS sample buffer at −20 °C. For immunoprecipitation of FLAG AS160 or FLAG control, transiently transfected HEK 293 cells were harvested as above, but with Triton X-100 containing buffer (50 mM Tris-HCl, pH 7.5, 150 mM NaCl, 0.5% Triton X-100, 1 mM EDTA, and 10% glycerol) containing Complete protease inhibitor mixture and phosphatase inhibitors (2 mM sodium orthovanadate, 1 mM sodium pyrophosphate, 10 mM sodium fluoride). FLAG AS160 or FLAG control were captured with FLAG antibody and protein G beads for 2 h at 4 °C. Immunoprecipitates were washed extensively and kept in 2× SDS sample buffer at −20 °C.

Subcellular Fractionation—After stimulation with insulin, 3T3-L1 adipocytes were washed with ice-cold PBS and harvested in ice-cold HES buffer (20 mM HEPES, pH 7.4, 1 mM EDTA, 250 mM sucrose) containing Complete protease inhibitor mixture and phosphatase inhibitors (2 mM sodium orthovanadate, 1 mM sodium pyrophosphate, 10 mM sodium fluoride). The cells were lysed with 12 passes through a 22-gauge needle and 6 passes through a 27-gauge needle. Cell lysates were then centrifuged at 500 × *g* for 10 min at 4 °C to remove unbroken cells. The supernatant was centrifuged at 10,080 × *g* for 20 min at 4 °C to yield the following two fractions: the pellet fraction consisting of PM and mitochondria/nuclei, and the supernatant fraction consisting of cytosol, low density microsomes (LDM), and high density microsomes. The supernatant was then centrifuged at 15,750 × *g* for 20 min at 4 °C to obtain the pellet high density microsome fraction. The supernatant was again centrifuged at 175,000 × *g* for 75 min at 4 °C to obtain the cytosol fraction (supernatant) and the LDM fraction (pellet). To obtain the PM fraction, pellet from the first ultracentrifuge spin was resuspended in HES buffer containing phosphatase and protease inhibitors and layered over high sucrose HES buffer (20 mM HEPES, pH 7.4, 1 mM EDTA, 1.12 M sucrose) and centrifuged at 78,925 × *g* for 60 min at 4 °C. The PM fraction was collected above the sucrose layer, and the pellet was the mitochondria/nuclei fraction. All the fractions were resuspended in HES buffer containing phosphatase and protease inhibitors. Protein concentration for each fraction was performed using BCA assay. Samples were made up in SDS sample buffer and then kept at −20 °C.

Lipid Raft Preparation—Following stimulation with insulin, 3T3-L1 adipocytes were washed with ice-cold PBS. Cells were harvested in ice-cold MES buffer (25 mM MES, pH 6.0, 150 mM NaCl) containing Complete protease inhibitor mixture and phosphatase inhibitors (2 mM sodium orthovanadate, 1 mM sodium pyrophosphate, 10 mM sodium fluoride) and lysed with 12 passes through a 22-gauge needle and 6 passes through a 27-gauge needle at 4 °C. Cell lysates were then centrifuged at 500 × *g* for 10 min at 4 °C to remove unbroken cells. The pellet was discarded, and the supernatant was solubilized with Triton X-100 in a final concentration of 1% on ice for 60 min. Following solubilization, the lysate was centrifuged at 18,000 × *g* for 15 min at 4 °C. The supernatant collected was the Triton-soluble fraction. The pellet, which is the Triton-insoluble fraction, was washed with MES buffer and then resuspended in MES buffer containing 1% SDS. Protein concentration was determined with BCA assay, and samples were made up in SDS sample buffer and kept at −20 °C.

Quantitative GLUT4 Translocation Assay—HA-GLUT4 translocation to the plasma membrane was measured as described previously (22). Briefly, 3T3-L1 adipocytes stably expressing HA-GLUT4 in 96-well plates were starved for 2 h in serum- and bicarbonate-free DMEM containing 20 mM HEPES, pH 7.4, and 0.2% BSA. After stimulation, cells were fixed and immunolabeled with monoclonal anti-hemagglutinin antibody followed by Alexa488-labeled secondary antibody in the absence or presence of saponin to analyze the amount of HA-GLUT4 at the plasma membrane or the total HA-GLUT4 content, respectively.

Confocal Laser Scanning Microscopy—3T3-L1 fibroblasts were seeded and differentiated into adipocytes on glass coverslips. Cells were serum-starved for 2 h at 37 °C before stimulation with the indicated doses of insulin for 20 min. For some experiments, cells were pretreated with 10 μM Akti or 0.1% DMSO for 15 min before insulin stimulation. After stimulation, cells were washed in ice-cold PBS, fixed with 3% paraformaldehyde, and quenched with 50 mM glycine. Cells were then blocked and permeabilized in 2% BSA and 0.1% saponin in PBS and labeled for activated Akt using rabbit monoclonal Ser(P)-473 Akt antibody. Primary antibody was detected with anti-rabbit Cy2-conjugated secondary antibody. Optical sections were obtained through scans for Cy2 using the Leica TCS SP confocal laser scanning microscope using a 63× 1.32 oil lens. For quantification, random images of Ser(P)-473 Akt at the base of the cells were collected with the same confocal settings.

Images were analyzed using the Region detector software, and the mean fluorescence was measured.

Fixed Cell Total Internal Refection Fluorescence (TIRF) Microscopy—3T3-L1 adipocytes were seeded in cloning rings attached to 42-mm coverslips. Following stimulations, cells were fixed with 3% paraformaldehyde and quenched with 50 mM glycine. Cells were then blocked and permeabilized in 2% BSA and 0.1% saponin in PBS and labeled for activated Akt using rabbit monoclonal Ser(P)-473 Akt antibody. Primary antibody was detected with anti-rabbit Alexa488-conjugated secondary antibody. Cells were imaged in PBS containing 5% glycerol and 2.5% 1,4-diazabicyclo[2-2-2]octane as described previously (23) using a Zeiss Axiocam MRm. Cells were randomly selected by bright field illumination prior to TIRF imaging, and images were analyzed with ImageJ software.

Modeling—The data from the experiments was quantified and normalized relative to the maximal response (long time or maximal dose). All data from all experiments were combined as a single data set to be fitted using nonlinear regression to obviate the need to weigh the different time/dose points.

Time courses were fitted to a single exponential rise, $y = (1 - p)\exp(-Kt) + 1$, where t is time; y is the level of the phosphorylation relative to the long term level; p is the initial value of phosphorylation (again relative to the long term level), and K is the rate. The half-time of the process was also determined as $H = \ln 2/K$.

The dose-response data were fitted to a logistic curve, $y = a/((1 - a)\exp(-rx) + a)$, where x is the dose; a is the initial (zero dose) phosphorylation level, relative to the maximal (infinite dose) phosphorylation level; and r is the rate. The dose at which the half-maximal response is observed, ED_{50}, is defined as shown in Equation 1,

$$ED_{50} = \frac{1}{r}\ln\left(\frac{1 + a}{a}\right) \quad \text{(Eq. 1)}$$

Hierarchical clustering was performed across either the dose variables, r, ED_{50}, and a, the temporal variables, K, H, and p, or both to group the different components.

The values of the variables were normalized, converting all values in the data set to use the same proportional scale, with zero mean and an S.D. of 1. The distance between every pair of components in the data set, the dissimilarity matrix, was determined. For this study a "city block" metric was employed, such that the distance between components r and s was defined as shown in Equation 2,

$$d_{rs} = \sum_{j=1}^{n} |z_{rj} - z_{sj}| \quad \text{(Eq. 2)}$$

where z_{rj} and z_{sj} are the normalized values of the jth variable of components r and s, respectively, and n is the total number of variables over which clustering is determined. The dissimilarity matrix was then analyzed to create a hierarchical cluster tree. The distance from one cluster of objects to another cluster of objects was defined as the unweighted average of the distances between individual objects in different clusters. Ultimately in hierarchical clustering, all clusters are combined. We then determined where to cut the hierarchical tree into clusters, either by determining a maximum distance separating members of a single cluster or alternatively specifying the number of clusters.

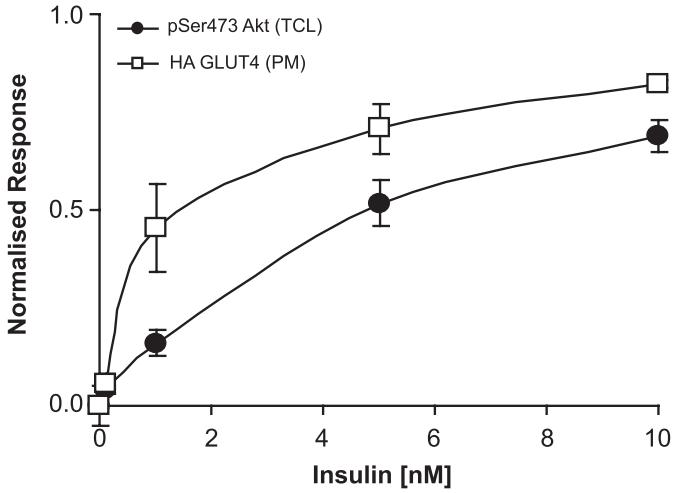

FIGURE 1. **Lack of correspondence between Akt phosphorylation and GLUT4 translocation.** Insulin dose-response of Ser(P)-473 Akt from the TCL and HA-GLUT4 translocation to the PM in 3T3-L1 adipocytes are shown. HA-GLUT4-expressing 3T3-L1 adipocytes were serum-starved for 2 h and stimulated with indicated dose of insulin for 20 min. Total cell lysates were immunoblotted with Ser(P)-473 Akt antibody. The amount of HA-GLUT4 at the plasma membrane was determined by anti-hemagglutinin fluorescence immunolabeling of nonpermeabilized cells and expressed as percentage of total cellular HA-GLUT4, determined by labeling of permeabilized cells. This was then normalized, such that 0 represents the basal level, and 1 represents the maximal response. ($n = 3$).

Statistical Analysis—Data are expressed as means ± S.D. p values were calculated by two-tailed Student's t test using Microsoft Office Excel 2003.

RESULTS

Dose and Kinetic Characteristics of Akt Signaling in 3T3-L1 Adipocytes—Given that Akt is necessary and sufficient in mediating GLUT4 translocation, one would expect to see a strong relationship between GLUT4 translocation and Akt phosphorylation. However, as illustrated in Fig. 1, we observed a poor relationship between insulin-regulated HA-GLUT4 translocation and total cellular Akt phosphorylation in 3T3-L1 adipocytes. This is most clearly represented by the difference in the ED_{50}, the dose that produces 50% of the maximal response, defining its sensitivity, and r, the dose rate constant, a measure of the dynamic range of the response (supplemental Table 1), which were found by fitting the data (see under "Experimental Procedures"). We next wanted to determine whether this shift in the behavior of Akt with respect to one of its major biological targets, GLUT4, is an intrinsic feature of all components in the insulin-signaling network. Alternatively, this may underpin a switch-like behavior of Akt or it may indicate that Akt is not the major regulator of insulin-regulated GLUT4 translocation. To test this, we selected a range of components in the insulin-signaling cascade, including phosphorylation of Akt at Thr-308 and Ser-473, putative Akt substrates (Ser(P)-9 GSK3, Thr(P)-642 AS160, Ser(P)-588 AS160, and Thr(P)-1462 TSC2), substrates located further downstream of Akt (Thr(P)-389 S6

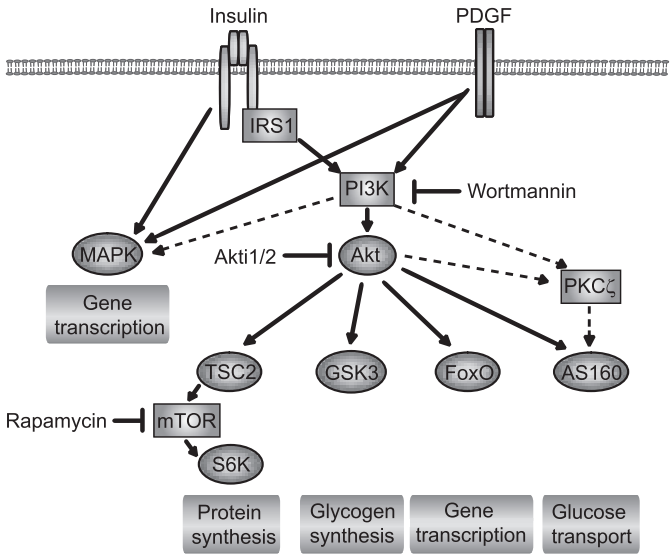

FIGURE 2. **Schematic diagram of signaling components under investigation.** A schematic of insulin- and PDGF-signaling pathways is shown. Activation of insulin or PDGF receptors triggers the activation of two pathways, p42/p44 MAPK and a PI 3-kinase (*PI3K*)-dependent pathways. Insulin activates PI 3-kinase via IRS1 adaptor proteins, whereas PDGF engages PI 3-kinase directly through PDGF receptor. Active PI 3-kinase then triggers the activation of atypical PKCζ and Akt. Akt then phosphorylates and activates its various downstream targets, AS160, GSK3, FoxO, and TSC2, mediating different cellular processes. Signaling components under investigation in this study are represented by *ovals*. S6K, S6 kinase ; *mTOR*, mammalian target of rapamycin.

kinase), or a substrate that is located on a separate branch of the insulin-signaling network (p42/p44 MAPK), as shown in Fig. 2. These phospho sites represent key regulatory sites in each of these molecules, and so this should provide a sensitive index of the activity of each component. Phospho-specific antibodies as well as antibodies against nonphosphorylated sites against each of these components were either produced in-house or obtained from commercial sources and were highly specific for their respective targets in 3T3-L1 adipocytes (see Fig. 3).

Comparison of the dose-response curves for each of these components revealed that the ED_{50} value (see under "Experimental Procedures") for insulin-stimulated Akt phosphorylation was of the order of 6 nM, whereas the ED_{50} value for insulin-stimulated Akt substrate phosphorylation was less by an order of magnitude (Fig. 3, *A* and *B*, and supplemental Table 1). The ED_{50} value of insulin-stimulated HA-GLUT4 translocation (0.94 nM) was more closely aligned with that of Thr(P)-642 AS160 (0.93 nM), the major Akt substrate implicated in this pathway (24), than of Akt itself. Hence, these data suggest that phosphorylation of AS160 at Thr(P)-642 rather than Akt is a better predictor of biological outcome. It is unlikely that this reflects a technical limitation in the Akt measurements as several other components (S6 kinase, p42/p44 MAPK, and Ser(P)-588AS160) displayed a similar ED_{50} value to Akt (Fig. 3, *A* and *B*, and supplemental Table 1).

Time course of response provides other variables that potentially describe component behavior. Among the Akt substrates, phosphorylation of Thr-642 AS160, Ser-9 GSK3β, and Thr-1462 TSC2 were very fast reaching their half-maximal value at ~15 s (Fig. 3, *C* and *D*, and supplemental Table 1). FoxO was somewhat slower possibly due to its nuclear localization (25). Notably, phosphorylation of Thr-389 S6 kinase, p42/p44 MAPK, and Ser-588 AS160 was very slow and in some cases not even showing a significant response until 5 min of insulin stimulation. However, unlike that observed for the dose-response studies, the time course of phosphorylation of Akt at both Thr-308 and Ser-473 was more akin to the Akt substrates (Fig. 3, *C* and *D*, and supplemental Table 1). Hence, this suggests that time course of response and dose-response analyses yield discrete behavioral aspects of signaling components. Nevertheless, time course data clearly resolved discrete behavioral differences particularly between different Akt substrates. We next wanted to examine the possibility that this temporal behavior was unique to insulin stimulation or a more generic feature of the signaling pathway *per se*. A distinguishing feature of the insulin receptor compared with other growth factor receptors is that it utilizes IRS1 as a scaffold to recruit and activate PI 3-kinase, whereas the PDGFR does so directly, bypassing IRS1 (see Fig. 2). Hence, we next engineered 3T3-L1 adipocytes to overexpress the PDGFR facilitating PDGF-dependent activation of GLUT4 translocation to a similar extent to that seen with insulin (data not shown). The time courses of the phosphorylation of the different components in response to insulin and PDGF are shown in Fig. 3, *C* and *D*.

We next wanted to analyze these findings using a quantitative approach. As described under "Experimental Procedures," the dose-response curves were fitted to obtain the dose-response variables, *i.e.* the ED_{50} value, the rate (r), and the basal phosphorylation level (a), and the time courses were fitted to obtain the temporal variables, *i.e.* half-time, the rate (k), and the initial phosphorylation level (p) (supplemental Table 1). These variables were then used to determine the relative similarity of the different components using hierarchical clustering (see "Experimental Procedures"). If we restricted the clustering to only the dose-response variables, then two major clusters were formed (Fig. 4*A*), which were consistent with the qualitative observations of the data above. The first cluster was composed of the Akt substrates (Thr(P)-642 AS160, Ser(P)-9 GSK3, Ser(P)-256 FoxO, and Thr(P)-1462 TSC2) together with HA-GLUT4 translocation. The second cluster was composed of Thr(P)-308 Akt, Ser(P)-473 Akt, p42/p44 MAPK, Ser(P)-588 AS160, and Thr(P)-389 S6 kinase. If both dose-response and temporal variables were used, this relationship was not significantly altered (Fig. 4*B*), indicating that the major features of these distinct clusters are dominated by the dose-response behavior. Hierarchical clustering of the dynamic response to insulin using the temporal variables alone segregated the components into two major clusters (with two outliers) (Fig. 4*C*). However, the two clusters were not identical to that achieved using the dose-response variables, as indicated in Fig. 4*A*. The Akt substrates that fell into a single cluster using dose-response variables were widely distributed among all clusters using temporal variables (as indicated by the color coding in Fig. 4*C*). Temporal variable clustering is, however, useful when comparing the response of the system to different types of stimuli, for instance to insulin and PDGF. Comparing the temporal clustering of the response to PDGF (Fig. 4*D*) with that of insulin (Fig. 4*C*), we observed a similar distribution of signaling components, with the only notable exception being Thr(P)-1462

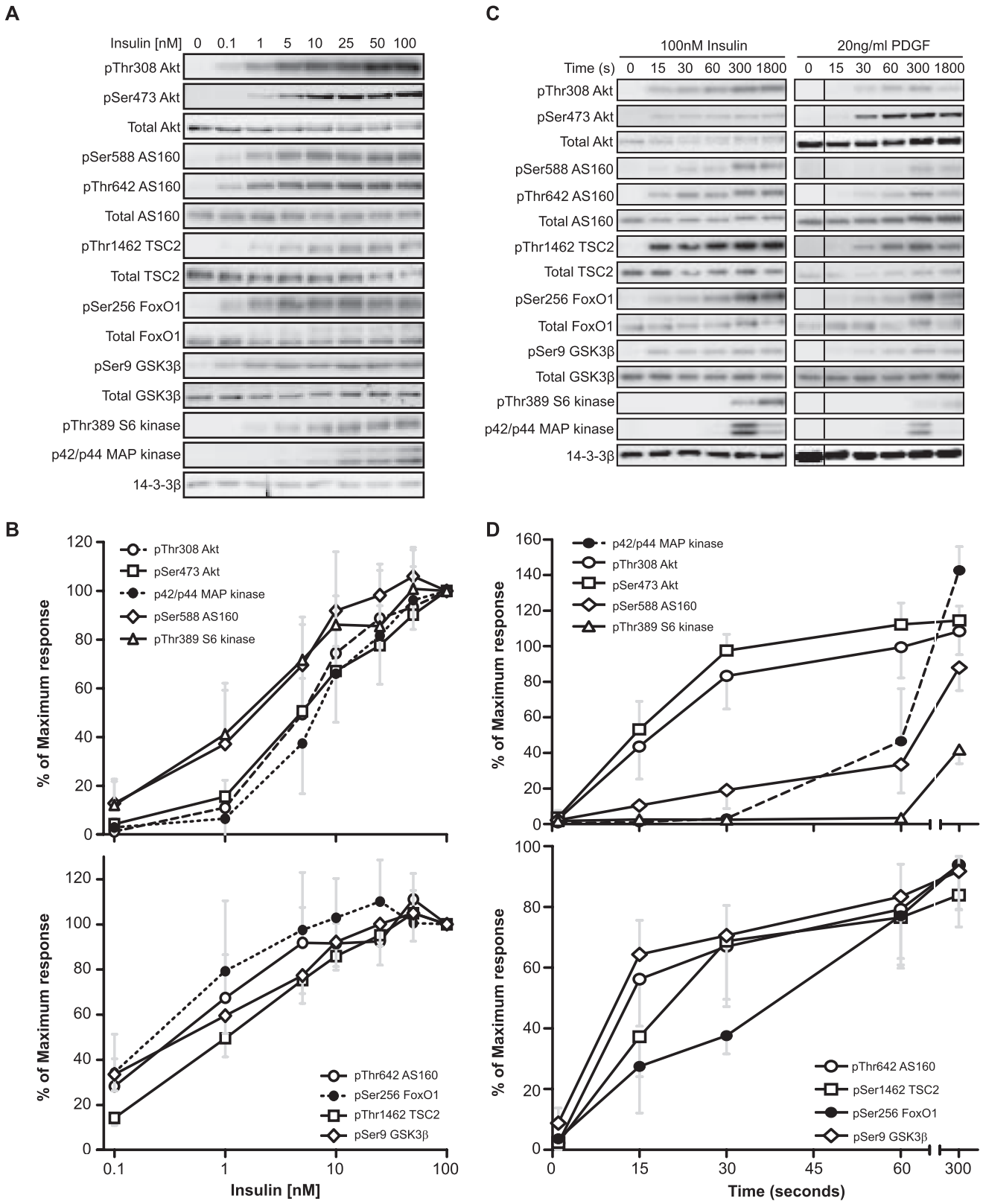

FIGURE 3. **Dose response and time course of insulin and PDGF signaling in 3T3-L1 adipocytes.** *A,* dose response of insulin signaling. 3T3-L1 adipocytes were serum-starved for 2 h and treated with different doses of insulin for 20 min. Total cell lysates were immunoblotted with antibodies raised against a panel of insulin-signaling components. Immunoblots are from a representative experiment ($n = 7–9$). *B,* signaling components were assigned into two different clusters based on their dose-response profiles. The *x* axis is $\log_{10}$ of the insulin dose, and the *y* axis is percentage of maximum response normalized to 100 nM insulin. Results are displayed as means ± S.D. ($n = 7–9$). *C,* time course of insulin and PDGF signaling. 3T3-L1 adipocytes or human PDGF receptor expressing 3T3-L1 adipocytes were serum-starved for 2 h and treated with either 100 nM insulin or 20 ng/ml PDGF for indicated periods of time. Total cell lysates were immunoblotted with antibodies raised against a panel of insulin-signaling components. Immunoblots are from a representative experiment (Insulin time course $n = 3$; PDGF time course $n = 2$). *D,* time course of various insulin-signaling components expressed as a maximum response of 30 min insulin stimulation. Results are displayed as means ± S.D.

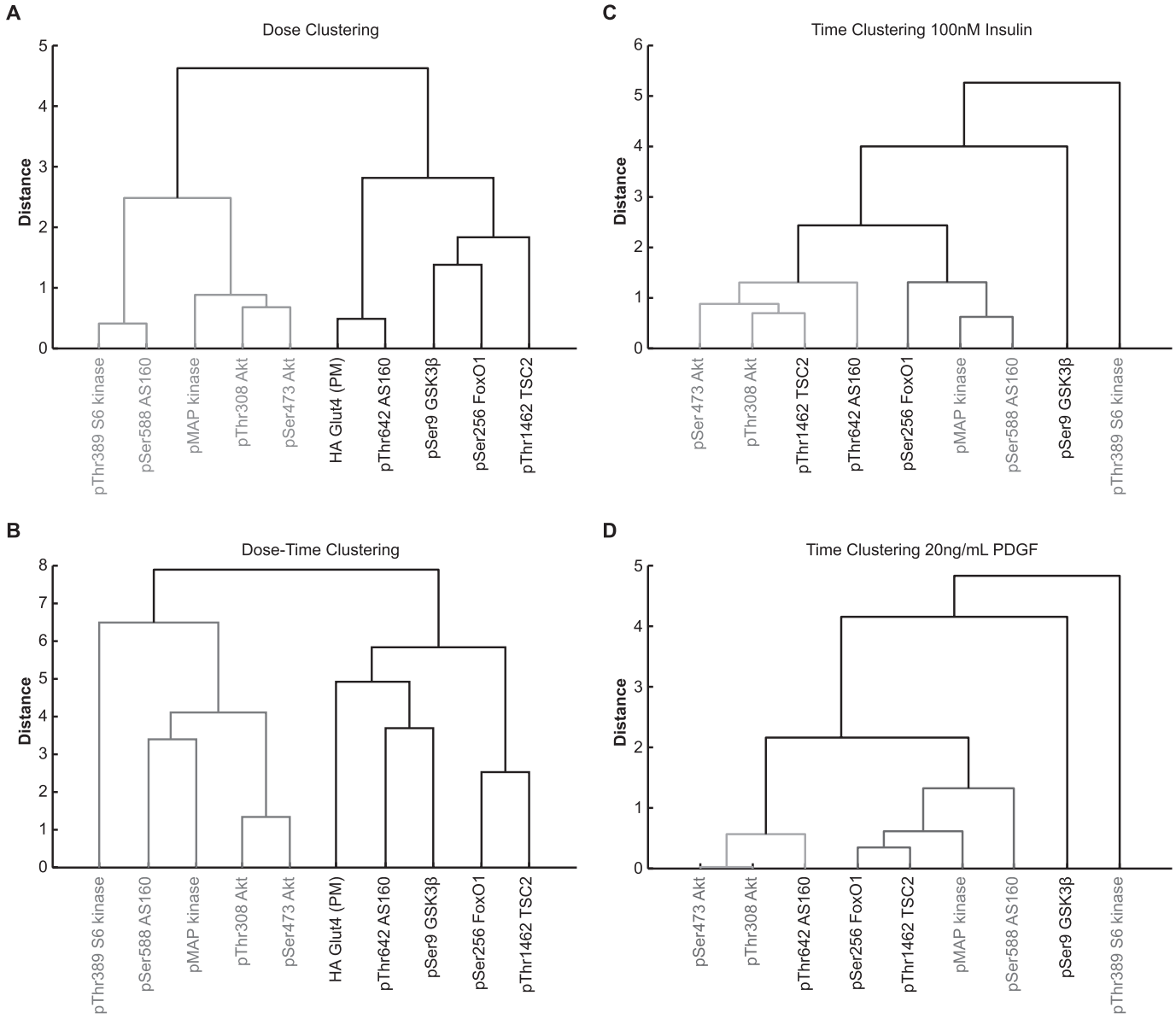

FIGURE 4. **Cluster analysis of dose-response and/or kinetics of insulin- and PDGF-stimulated Akt signaling.** *A,* clustering of insulin response over dose variables. The two major clusters are shown as follows: Akt substrates and HA-GLUT4 at the PM (*black*) and other signaling components (*gray*). *B,* clustering of insulin response over dose and temporal variables. The two major clusters are shown as follows: Akt substrates and HA-GLUT4 at the PM (*black*) and other signaling components (*gray*). Note these are identical in grouping to that of *A*. *C,* clustering of insulin response over temporal variables. Two major groups of phosphorylated signaling components were found, shown in *light gray* and *dark gray*, along with two outliers. The two groups from the dose variable clustering in *A* and *B* are shown in *black* and *gray* on the component labels. *D,* clustering of PDGF response over temporal variables. As in *C,* two major groups of phosphorylated signaling components were found, shown in *light gray* and *dark gray*, along with two outliers. The only difference in grouping to *C* is that of Thr(P)-1462 TSC2. Again, the two groups from the dose variable clustering in *A* and *B* are shown in *black* and *gray* on the component labels.

TSC2. This suggests that the temporal behavior of the signaling components is embedded within the canonical PI 3-kinase/Akt network and independent of IRS1.

Insulin Dose Response of Active Akt on the Plasma Membrane—The data described above indicate that the temporal and dose characteristics of Akt substrate phosphorylation are a better predictor of biological outcome, in this case GLUT4 translocation, than phosphorylation of the total cellular pool of Akt (Fig. 4*B*). This implies that Akt phosphorylation, at least as measured here, is lacking one or more key regulatory features of kinase activity *in vivo*. Recent evidence suggests that subcellular location may be an important determinant of Akt specificity (26, 27), so we next utilized morphological and biochemical methods to dissect this aspect of Akt function. Confocal (Fig. 5*A*) and TIRF (Fig. 5*B*) microscopy revealed that in response to insulin there was a significant increase in Akt phosphorylation at the PM in 3T3-L1 adipocytes. This labeling was specific being inhibited by the specific Akt inhibitor Akti-1/2 (Fig. 5, *C* and *D*). Notably, measurement of Akt phosphorylation at the PM using either confocal or TIRF microscopy at different insulin concentrations revealed a very different pattern to that observed for Akt phosphorylation measured biochemically in whole cell lysates (Fig. 5*E*). Hierarchical clustering over the dose variables revealed that Akt phosphorylation spatially confined to the PM

behaved like GLUT4 translocation and Thr(P)-642 AS160 phosphorylation and was found in a separate cluster to total cellular Akt phosphorylation (Fig. 5*F*).

Highly Phosphorylated Pool of AS160 on the Plasma Membrane—The clustering data described above made several predictions about the topology of the Akt network. First, the

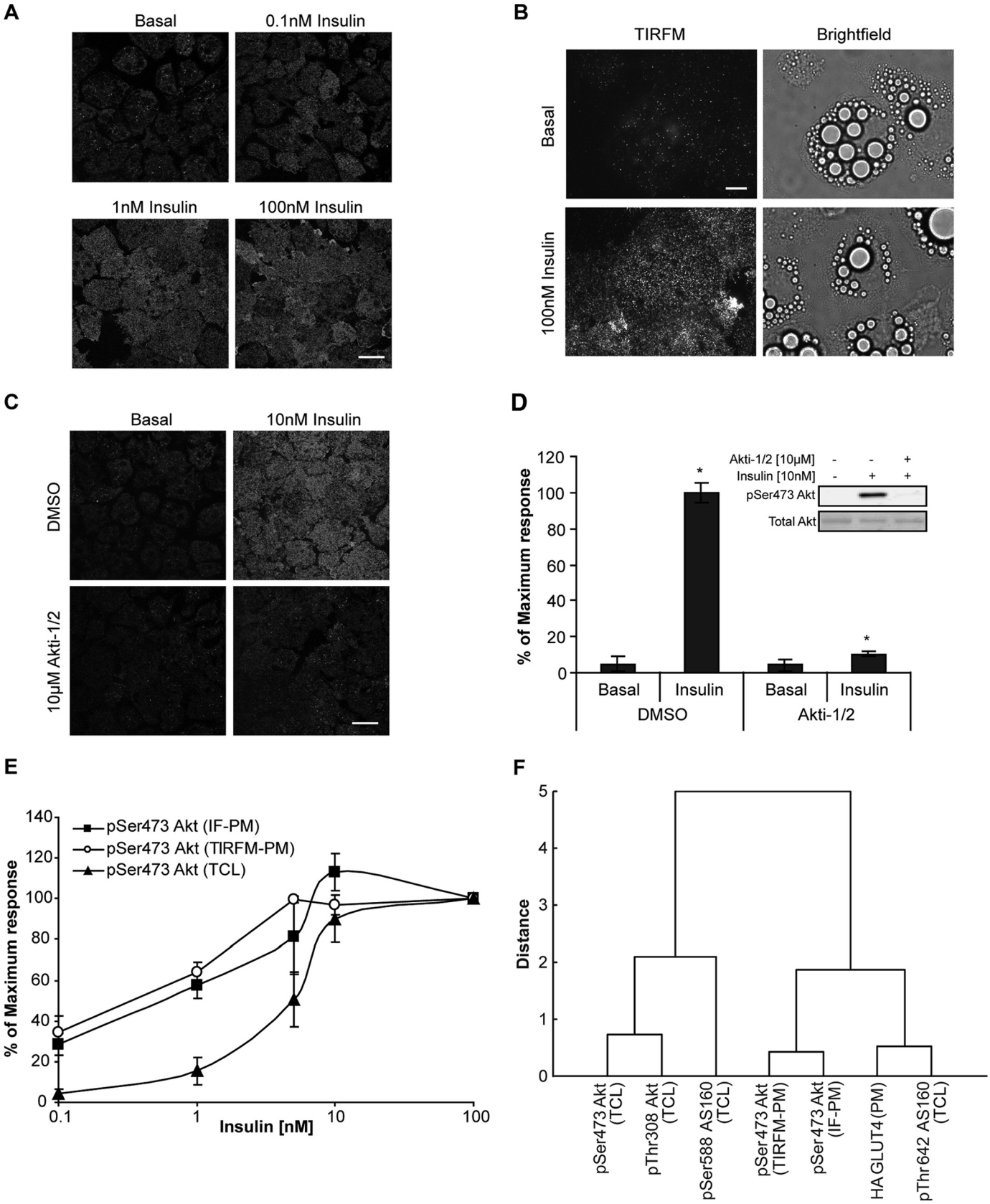

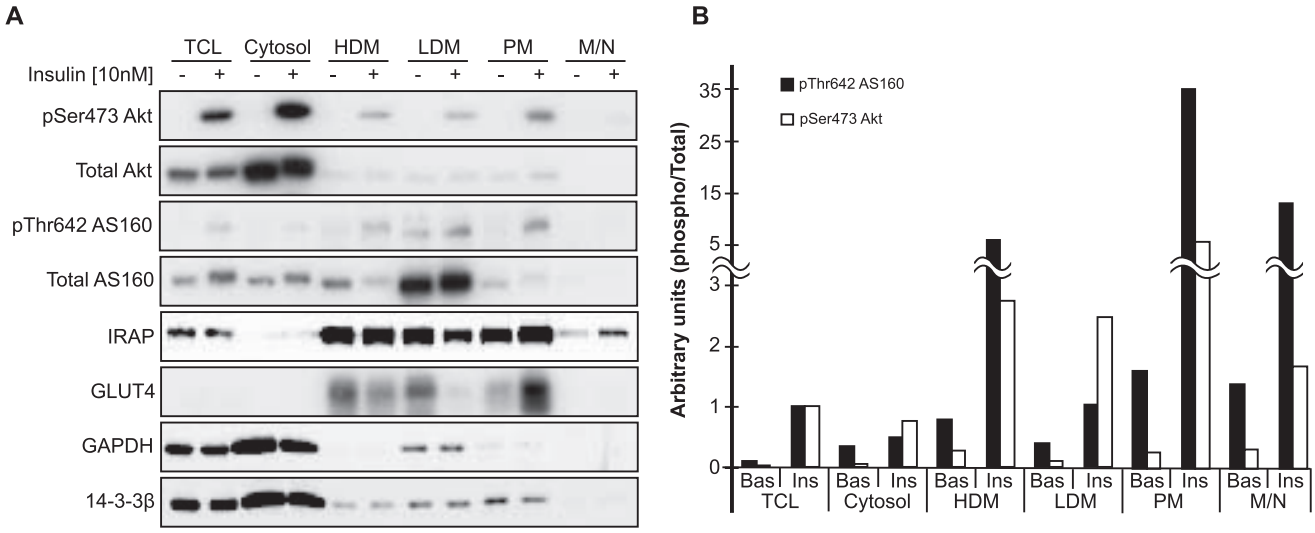

FIGURE 6. **Phosphorylated AS160 is concentrated at the plasma membrane.** *A,* 3T3-L1 adipocytes were serum-starved for 2 h and treated with 10 nM insulin for 20 min. Cells were then fractionated to obtain different subcellular fractions, TCL, cytosol, high density microsomes (*HDM*), low density microsomes (*LDM*), plasma membranes (*PM*), and mitochondria/nuclei (*M/N*). Fractions were then subjected to Western blot analysis with Ser(P)-473 Akt, total Akt, Thr(P)-642 AS160, total AS160, IRAP, GLUT4, glyceraldehyde-3-phosphate dehydrogenase (*GAPDH*), and 14-3-3β antibodies. *B,* quantification of *A.* Specific activity of Ser(P)-473 Akt and Thr(P)-642 AS160 was from various fractions normalized against insulin stimulation of the TCL. *Ins*, insulin; *Bas*, basal.

highly significant relationship between Akt activation at the PM and the phosphorylation of several key downstream targets, including AS160, raises the possibility that phosphorylation of these substrates occurs at the PM. Second, the relatively poor relationship between Akt phosphorylation of the same substrate AS160 at two separate sites (Thr-642 and Ser-588) suggests a nonuniformity in access of Akt to distinct domains within this molecule that are not immediately evident from published data (24, 28). To further investigate these issues, we employed a biochemical approach involving a well established subcellular fractionation protocol to study the compartmental organization of Akt together with its substrates. The majority of insulin-stimulated phospho-Akt was found in the cytosol with lower levels identified in membrane fractions (high density microsomes, LDM, PM, and mitochondria/nuclei) (Fig. 6*A*). The specific activity of phospho-Akt was highest in the PM fraction (Fig. 6*B*). These data are consistent with the morphological data showing that there is a pool of active Akt enriched in the PM (Fig. 5). Insulin-stimulated Thr(P)-642 AS160 was also highly enriched in the PM suggesting that this is likely the site where this substrate is both phosphorylated by Akt and possibly where it mediates its principal function. Consistent with previous data (21), the majority of immunoreactive AS160 was in the LDM fraction both in the absence and presence of insulin (Fig. 6*A*), suggesting that a relatively small pool of this protein is phosphorylated at Thr-642 even in response to maximum insulin stimulation. To confirm this observation, we next performed immunoprecipitation using the anti-Thr(P)-642 AS160 antibody (Fig. 7*A*). This resulted in efficient isolation of the Thr(P)-642 form of the AS160 as indicated by the fact that the flow-through fraction was almost completely depleted of this antigen. However, a large proportion of immunoreactive AS160 was found in the flow-through consistent with the fact that a relatively small pool of AS160 is phosphorylated at the Thr-642 site (Fig. 7*A*). Surprisingly, the majority of insulin-stimulated Ser(P)-588 AS160 was also found in the flow-through indicating that phosphorylation at Thr(P)-642 and Ser(P)-588 is mutually exclusive. This was reminiscent of our cluster analysis described above (Fig. 4*A*) where insulin-dependent phosphorylation of AS160 at Ser-588 was found in a discrete cluster from all other Akt substrates. Intriguingly, the dose-response cluster analysis placed AS160 Ser-588 phosphorylation closest to S6 kinase phosphorylation than to any other signaling component (Fig. 4*A*). Hence, we next tested the hypothesis that mammalian target of rapamycin or S6 kinase may phosphorylate AS160 at

FIGURE 5. **Akt at the plasma membrane correlates with GLUT4 trafficking.** *A,* insulin dose response of Ser(P)-473 Akt at the cell surface. 3T3-L1 adipocytes were serum-starved for 2 h and treated with different doses of insulin for 20 min. Cells were fixed and immunolabeled with Ser(P)-473 Akt followed by Cy2-conjugated secondary antibody. Confocal slice images were taken at the base of the cell. Images are from a representative experiment ($n = 3$; 30–50 images per condition in each experiment). *Scale bar,* 40 μm. *B,* insulin dose-response of Ser(P)-473 Akt at the cell surface. 3T3-L1 adipocytes were serum-starved for 2 h and treated with different doses of insulin for 20 min. Cells were fixed and immunolabeled with Ser(P)-473 Akt followed by Alexa488-conjugated secondary antibody. Cells were then imaged by TIRFM. Representative images are shown ($n = 2$; 30–50 images per condition in each experiment). *Scale bar,* 10 μm. *C,* 3T3-L1 adipocytes were serum-starved for 2 h and treated with either 0.1% DMSO or 10 μM Akti-1/2 for 15 min before stimulation with 10 nM insulin for 20 min. Cells were fixed, and active Akt was immunolabeled with anti-Ser(P)-473 Akt antibody in combination with Cy2-conjugated secondary antibody in permeabilized cells. Images were taken as in *A*. Images are from a representative experiment ($n = 3$; 30–50 images per condition in each experiment). *Scale bar,* 40 μm. *D,* quantification of *C*. The amount of Ser(P)-473 Akt at cell surface was determined using the region detector program. Results are displayed as means ± S.D. *, $p < 0.05$, insulin-treated *versus* insulin and Akti-1/2 treatment, Student's *t* test ($n = 3$). *Inset* is the total cell lysates of 3T3-L1 adipocytes immunoblotted with antibodies against Ser(P)-473 Akt and total Akt. *E,* insulin dose response of Ser(P)-473 Akt from the TCL, IF-PM, and TIRFM-PM expressed as a maximum response of 100 nM insulin stimulation. Results are displayed as means ± S.D. *F,* clustering of insulin response over dose variables for signaling components from the TCL (Thr(P)-308 Akt, Ser(P)-473 Akt, Ser-588 AS160, and Thr-642 AS160), Ser(P)-473 (*IF-PM*), Ser(P)-473 (*TIRFM-PM*), and HA-GLUT4 (*PM*). Note that although Ser(P)-588 AS160 is clustered with the TCL Akt components, Thr(P)-642 AS160 clusters with both the Akt components at the PM as well as HA-GLUT4 at the PM.

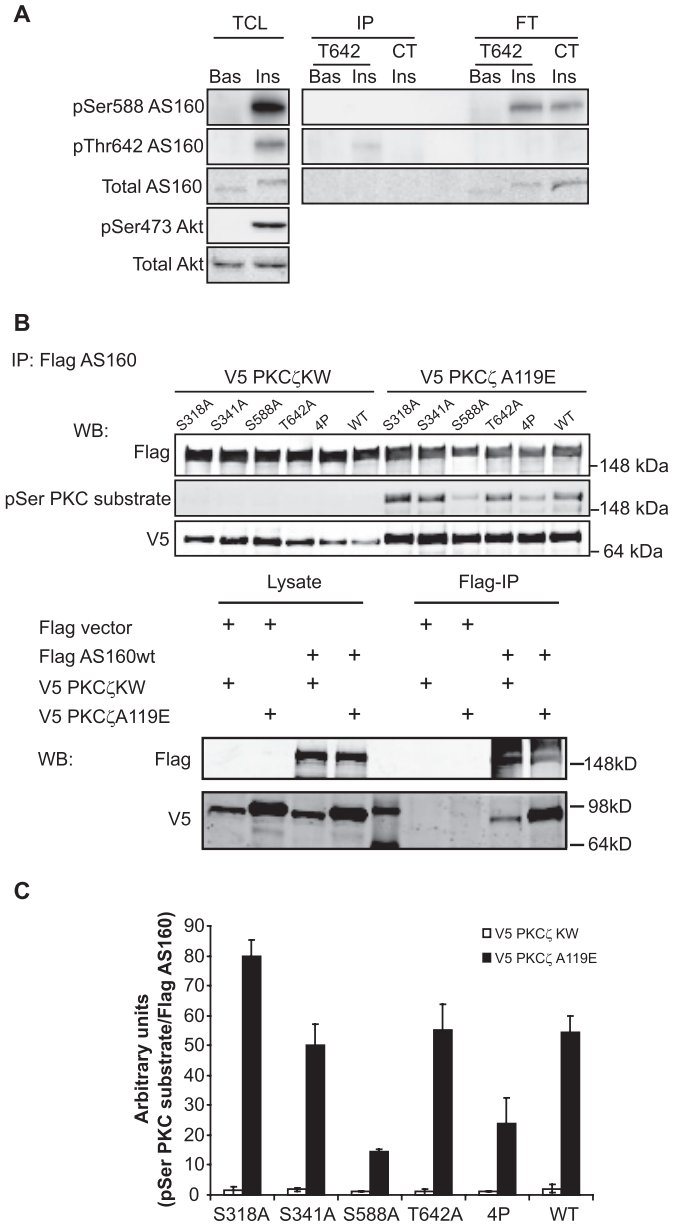

FIGURE 7. **Differences in phosphorylation in Ser-588 and Thr-642 on AS160.** *A*, 3T3-L1 adipocytes were serum-starved for 2 h and treated with 100 nM insulin for 20 min. Cell lysates were prepared, and Thr-642-phosphorylated AS160 was immunoprecipitated (*IP*) with specific Thr(P)-642 AS160 rabbit antibody. A nonimmunized rabbit IgG (*CT*) was used as control for immunoprecipitation using insulin-stimulated lysates. The immune complexes (*IP*) and the flow-through (*FT*) were then immunoblotted with Ser(P)-588 AS160, Thr(P)-642 AS160, and total AS160 antibodies. TCL were also immunoblotted for Ser(P)-588 AS160, Thr(P)-642 AS160, total AS160, Ser(P)-473 Akt, and total Akt. *B*, HEK 293 cells were transfected with either V5 PKCζ A119E (dominant active) or V5 PKCζ KW (dominant negative), in combination with different mutants of FLAG-tagged AS160 (S318A, S341A, S588A, T642A, 4P, or wild type (*wt*)) or FLAG vector control. Cell lysates were prepared, and FLAG AS160 wild type or mutants or FLAG control were immunoprecipitated with FLAG antibody. The immune complexes were then immunoblotted with FLAG, V5, and phospho-Ser PKC substrate antibodies. *WB*, Western blot. *C*, quantification of *B*. The amount of phosphorylation was normalized against immunoprecipitated FLAG AS160. Results are displayed as means ± S.D. ($n = 2$). *WT*, wild type.

Ser-588 *in vivo* using the mammalian target of rapamycin inhibitor rapamycin and other kinase inhibitors. Whereas the specific Akt inhibitor Akti-1/2 blocked AS160 Ser-588 phosphorylation, no inhibition was observed with rapamycin, in contrast to S6 kinase phosphorylation that is blocked by both inhibitors (supplemental Fig. 1).

Based upon the differential clustering between Ser(P)-588 AS160 and other Akt substrates (Fig. 4*A*), we reasoned that phosphorylation at Ser-588 may be regulated by an alternate kinase. Because atypical PKCs have been implicated in insulin action downstream of PI 3-kinase (29), we tested the hypothesis that they may regulate AS160 Ser-588 phosphorylation. As shown in Fig. 7*B*, we observed direct interaction between PKCζ (PKCζ A119E dominant active; PKCζ KW dominant negative) and AS160 as well as PKCζ-dependent phosphorylation of AS160. Intriguingly, mutation of the Ser-588 site but not mutation at other insulin-regulated sites on AS160 (24) resulted in almost complete abolition of PKCζ-mediated phosphorylation of AS160 (Fig. 7, *B* and *C*), whereas the interaction between these proteins was unaffected (Fig. 7*B*). Moreover, mutation of the Ser-588 site alone resulted in a similar loss of binding to the phospho-Ser PKC substrate antibody as that seen for the 4P AS160 mutant in which all four insulin-regulated phosphorylation sites have been mutated (Fig. 7, *B* and *C*) (24). Taken together, these data indicate that a minority of the AS160 pool is phosphorylated on Thr-642 upon maximum insulin stimulation and that this pool is distinct from that phosphorylated at Ser-588.

Concentration of Insulin Signaling in Detergent-insoluble Rafts—The PM is a heterogeneous organelle composed of lipid raft and nonraft domains (30). Some reports have suggested that lipid rafts represent signaling subdomains, so we next examined the distribution of the insulin-signaling pathway within these subdomains. Rather than isolate PM from 3T3-L1 adipocytes prior to separation of raft domains potentially running the risk of disrupting the architecture of these structures, we opted to use a more rapid method involving detergent insolubility. This relatively simple fractionation method was effective at isolating lipid rafts as indicated by the enrichment of caveolin, a marker for lipid rafts, in the Tx_{insol} fraction and enrichment of the cytosolic proteins 14-3-3β and Crk in the Tx_{sol} fraction (Fig. 8*A*). The specific activity of Ser(P)-473 Akt and Ser(P)-9 GSK3 was similar in these two fractions. However, both Thr(P)-642 AS160 and Ser(P)-588 AS160 were highly enriched in the Tx_{insol} fraction, but in contrast to Ser(P)-588 AS160, Thr(P)-642 AS160 was almost undetectable in the Tx_{sol} fraction (Fig. 8, *A* and *B*). These data show first that Thr(P)-642 AS160 is localized differently from other Akt substrates (Fig. 8 and data not shown) and second that there are distinct pools of AS160, highlighting the crucial role of compartmentalization in signal transduction.

DISCUSSION

Hierarchical clustering of the canonical PI 3-kinase/Akt pathway in 3T3-L1 adipocytes using dose and temporal variables reveals several novel topological features of this network. First, Akt substrates, including TSC2, GSK3, AS160, and FoxO, belonged to a distinct cluster that could be segregated from non-Akt substrates such as S6 kinase and p42/p44 MAPK. Second, a disparity was observed between phosphorylation of a range of Akt substrates and Akt itself, and this was resolved by considering the spatial localization of active Akt, implicating an important role for Akt at the PM. Third, Akt phosphorylation at the PM was highly clustered with AS160 phosphorylation

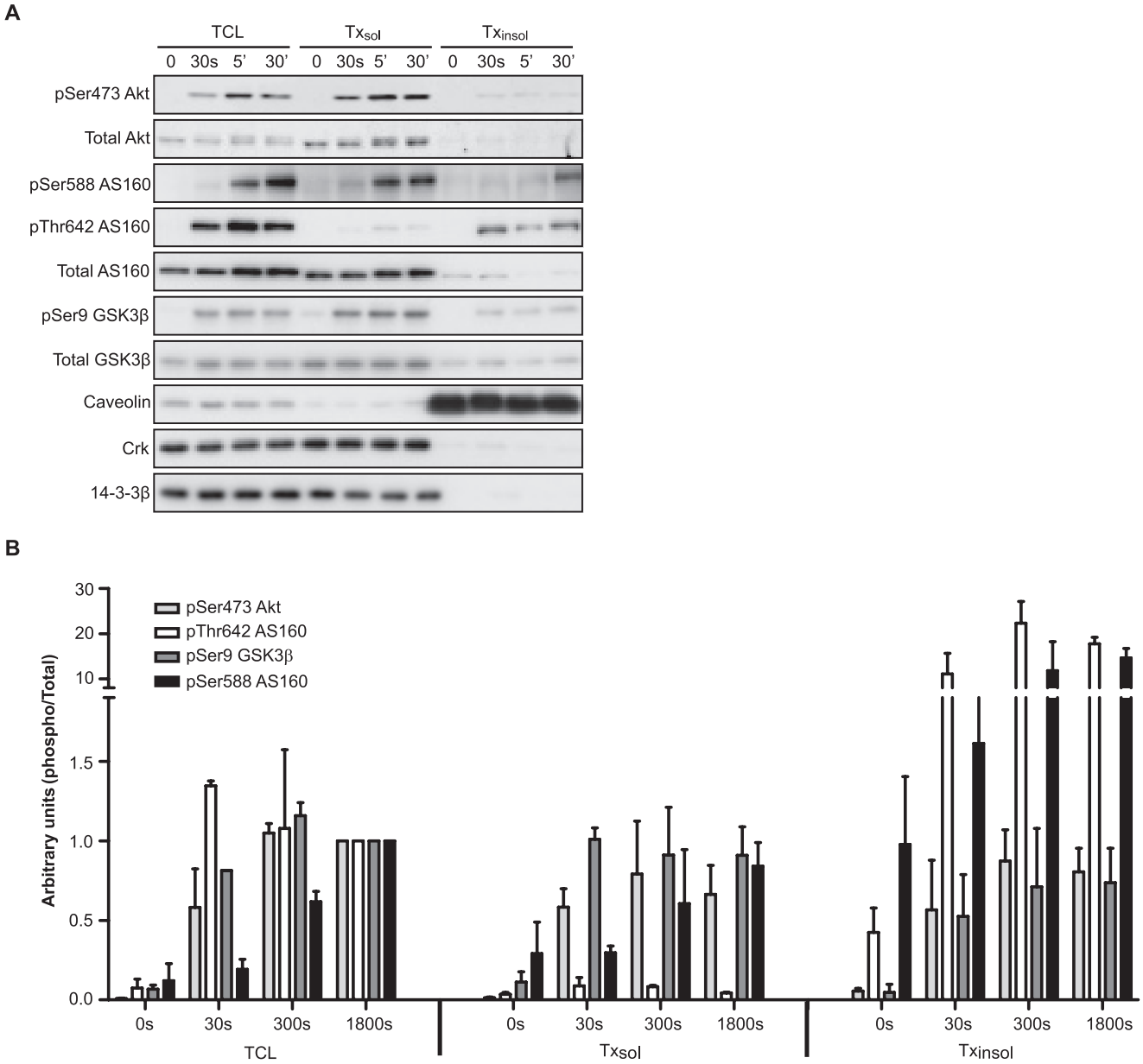

FIGURE 8. **Phospho-AS160 is concentrated in a detergent-insoluble fraction.** *A,* 3T3-L1 adipocytes were serum-starved for 2 h and treated with 100 nM insulin for the indicated period of times. Cells were then fractionated into Triton-soluble fraction (Tx_{sol}) or Triton-insoluble fraction (Tx_{insol}) fractions. TCL and the fractions were then subjected to Western blot analysis with Ser(P)-473 Akt, total Akt, Ser(P)-588 AS160, Thr(P)-642 AS160, total AS160, Ser(P)-9 GSK3β, total GSK3β, caveolin, Crk, and 14-3-3β antibodies. *B,* quantification of *A.* Specific activity of Ser(P)-473 Akt, Ser(P)-588 AS160, Thr-642 AS160, and Ser(P)-9 GSK3β from various fractions normalized against insulin stimulation (30 min) of the TCL. Results are displayed as means ± S.D. ($n = 2$).

at Thr-642 as well as with GLUT4 translocation providing independent evidence for a functional link between these components. Finally, phosphorylation of AS160 at an alternate putative Akt site, Ser-588 did not cluster with Thr-642 phosphorylation nor with other Akt substrates suggesting that this is not an Akt substrate. Further functional studies revealed that Ser-588 in AS160 is a substrate of atypical PKCζ and that phosphorylation at the Ser-588 and Thr-642 sites is mutually exclusive suggesting a sequential mode of regulation.

The starting point for these studies was that the ED_{50} for insulin-stimulated GLUT4 translocation in 3T3-L1 adipocytes was significantly less than that of insulin-stimulated Akt activation. This did not fit with the concept that the Akt pathway is necessary and sufficient for this particular biological action of insulin because if this were the case one would predict direct transmission between individual pathway components and thus a more predictable behavior of the pathway as a whole. This was borne out in analysis of a group of Akt substrates, which elicited behavior more analogous to GLUT4 translocation than to Akt phosphorylation itself. This discrepancy at the Akt node was resolved with the realization that Akt displays spatially restricted behavior in that Akt phosphorylation at the PM, but not in the whole cell lysate, was highly correlated with GLUT4 translocation. It is perhaps not surprising that a functional pool of Akt resides at the PM because this is where the enzyme is activated. As to whether this reflects preferential localization of a particular Akt isoform to the plasma membrane, as recently suggested by Gonzalez and McGraw (31), will

require further study. The observation that Akt phosphorylation at the PM is highly clustered with the phosphorylation of several Akt substrates raises the possibility that phosphorylation of these substrates may well occur at the PM or another restricted compartment. This conclusion was supported by subcellular fractionation studies, which showed an enrichment of the phospho-Akt substrates in the PM fraction. Consistent with the PM as a central location of the Akt node, it has been shown that selective targeting of Akt to the PM (32, 33) results in Akt activation concomitant with robust GLUT4 translocation and phosphorylation of AS160, GSK3, and S6 kinase.

Cluster analysis of multisite phosphorylation of AS160 further exemplified the utility of this approach for dissecting novel features of signaling pathways. Although phosphorylation of AS160 at Thr-642 was highly clustered with GLUT4 translocation, this was not the case for another putative Akt site at Ser-588. Further analysis revealed that phosphorylation of AS160 at Ser-588 is probably regulated by atypical PKCζ and not by Akt directly, and phosphorylation at Ser-588 and Thr-642 is mutually exclusive. This raises the possibility that AS160 regulation is more complex than previously realized involving either a multisite phosphorylation cascade or two functionally distinct pools of AS160. Phosphorylation of Thr-642 on AS160 is important for 14-3-3 binding and GLUT4 trafficking (20), and many agonists that regulate GLUT4 translocation induce phosphorylation at this site (28). On the other hand, this was not the case for Ser-588, and the importance of Ser-588 phosphorylation is still not well understood (28). It should also be noted that AS160 possesses several other regulated phosphorylation sites (34) that require more detailed analysis.

Despite the fact that the Akt substrates do cluster based on dose-response and time course variables, it was of interest that taking dose response alone into account, which tends to dominate this relationship, then among the four Akt substrates studied, the strongest link to GLUT4 translocation was with AS160. This is striking in view of the known role of AS160 in GLUT4 trafficking in 3T3-L1 adipocytes (21, 24). In contrast, FoxO, TSC2, and GSK3 regulate transcription, protein synthesis, and glycogen synthesis, respectively (4). Thus, it is of interest to discern other unique features of AS160 regulation that distinguish it from these other substrates. First, the specific activity of Thr(P)-642 AS160 in the PM was considerably higher than that of other substrates. Second, within the PM, Thr(P)-642 AS160 was confined to a detergent-insoluble subdomain as was a limited pool of active Akt. Finally, the stoichiometry of AS160 phosphorylation at Thr(P)-642 was very low with the majority of the protein being found in the LDM fraction. These observations highlight the fact that unlike other Akt substrates, such as FoxO, insulin regulation of AS160 is confined to a very discrete subpopulation of AS160 molecules. These data raise novel insights into the process as well as new questions concerning AS160 regulation. Previously, it was thought that AS160 functions by binding to intracellular GLUT4 vesicles in the absence of insulin and inhibiting a Rab required for GLUT4 trafficking with its Rab GTPase-activating protein (RabGAP) domain (21). Insulin-dependent phosphorylation of AS160 was suggested to inhibit its RabGAP activity, thus promoting Rab GTP loading and GLUT4 trafficking (21, 24). In this model, however, there is no *a priori* role for AS160 at the PM. Based on these data, we feel it is necessary to consider an alternative model where the major functional pool of AS160 resides in a specific location within the PM. This localization may serve to bring AS160 into proximity of a discrete pool of active Akt and possibly other molecules such as the putative Rab substrate. In this model, phosphorylation of AS160 may not only affect the RabGAP activity of AS160 but also its ability to act as an effector for vesicle docking and fusion with the PM, an event that might ultimately be linked to its GTPase-activating protein activity to recycle the components that underpin this process. It will be of interest to determine how AS160 and Akt are targeted to the discrete PM subdomain and as to whether these proteins form a complex at this site. Recent studies have identified Akt-binding proteins that may serve such a function. These include APPL1 (35) and ClipR-59 (27), both of which have been implicated in insulin action and GLUT4 trafficking. It is, however, clear from this study that the regulation of AS160 by Akt and that of other Akt substrates is distinct, which is consistent with the possibility that different Akt-binding proteins selectively tether the kinase to unique substrates. For example, endosomal partitioning of Akt by APPL1 appears to control phosphorylation of GSK3 but not TSC2 (36). In contrast, targeting of Akt to lipid rafts controls the phosphorylation of a different subset of substrates (26).

These studies validate the prediction that functionally linked intermediates in complex signal transduction networks display highly related behavior. This behavior can be mapped based upon analysis of a relatively simple set of variables that include the dose-response relationship and the kinetics of the response. By subjecting such data to hierarchical cluster analysis, it is feasible to make novel predictions about the topology and composition of signaling pathways. This study supports the emerging concept that subcellular localization plays a central role in determining the sensitivity, specificity, and kinetics of signaling that may skew interpretation of studies that have overlooked this parameter. In this context, we found that the dose response of Akt activation at the PM but not in the whole cell lysate correlates with GLUT4 translocation. Further studies are required to identify alternate Akt substrates in the PM that could play an important role in this process. These findings bring us a step closer to understanding the physiology of insulin action and how it might go awry.

Acknowledgments—We thank Dr. Gus Lienhard (Dartmouth Medical School, Dartmouth, NH) for providing the FLAG AS160 wild-type and 4P mutant plasmids; Dr. Jonathan Cooper (Fred Hutchinson Cancer Research Center, Seattle, WA) for providing PDGFR plasmid; Dr. Trevor Biden (Garvan Institute of Medical Research, Sydney, Australia) for providing PKCζ A119E and PKCζ KW plasmids; and Dr. Peter Shepherd (Symansis, Auckland, New Zealand) for generously providing Ser(P)-588 AS160 and Thr(P)-642 AS160 antibodies and the Akti1/2-specific inhibitor. We also thank Katarina Mele (CSIRO, Sydney, Australia) for developing the region detector software and Prof. Ted Kraegen and Dr. Mark Cowley for critically reading the manuscript (Garvan Institute of Medical Research, Sydney, Australia).

REFERENCES

1. Cantley, L. C. (2002) *Science* **296,** 1655–1657
2. Sarbassov, D. D., Guertin, D. A., Ali, S. M., and Sabatini, D. M. (2005)

Science **307,** 1098–1101
3. Hresko, R. C., and Mueckler, M. (2005) *J. Biol. Chem.* **280,** 40406–40416
4. Manning, B. D., and Cantley, L. C. (2007) *Cell* **129,** 1261–1274
5. Whiteman, E. L., Cho, H., and Birnbaum, M. J. (2002) *Trends Endocrinol. Metab.* **13,** 444–451
6. Kane, S., Sano, H., Liu, S. C., Asara, J. M., Lane, W. S., Garner, C. C., and Lienhard, G. E. (2002) *J. Biol. Chem.* **277,** 22115–22118
7. Cross, D. A., Alessi, D. R., Cohen, P., Andjelkovich, M., and Hemmings, B. A. (1995) *Nature* **378,** 785–789
8. Potter, C. J., Pedraza, L. G., and Xu, T. (2002) *Nat. Cell Biol.* **4,** 658–665
9. Kitamura, T., Kitamura, Y., Kuroda, S., Hino, Y., Ando, M., Kotani, K., Konishi, H., Matsuzaki, H., Kikkawa, U., Ogawa, W., and Kasuga, M. (1999) *Mol. Cell. Biol.* **19,** 6286–6296
10. Biggs, W. H., 3rd, Meisenhelder, J., Hunter, T., Cavenee, W. K., and Arden, K. C. (1999) *Proc. Natl. Acad. Sci. U.S.A.* **96,** 7421–7426
11. White, M. F. (1998) *Mol. Cell. Biochem.* **182,** 3–11
12. Knight, Z. A., Gonzalez, B., Feldman, M. E., Zunder, E. R., Goldenberg, D. D., Williams, O., Loewith, R., Stokoe, D., Balla, A., Toth, B., Balla, T., Weiss, W. A., Williams, R. L., and Shokat, K. M. (2006) *Cell* **125,** 733–747
13. Foukas, L. C., Claret, M., Pearce, W., Okkenhaug, K., Meek, S., Peskett, E., Sancho, S., Smith, A. J., Withers, D. J., and Vanhaesebroeck, B. (2006) *Nature* **441,** 366–370
14. Cho, H., Mu, J., Kim, J. K., Thorvaldsen, J. L., Chu, Q., Crenshaw, E. B., 3rd, Kaestner, K. H., Bartolomei, M. S., Shulman, G. I., and Birnbaum, M. J. (2001) *Science* **292,** 1728–1731
15. Jiang, Z. Y., Zhou, Q. L., Coleman, K. A., Chouinard, M., Boese, Q., and Czech, M. P. (2003) *Proc. Natl. Acad. Sci. U.S.A.* **100,** 7569–7574
16. Katome, T., Obata, T., Matsushima, R., Masuyama, N., Cantley, L. C., Gotoh, Y., Kishi, K., Shiota, H., and Ebina, Y. (2003) *J. Biol. Chem.* **278,** 28312–28323
17. Hoehn, K. L., Hohnen-Behrens, C., Cederberg, A., Wu, L. E., Turner, N., Yuasa, T., Ebina, Y., and James, D. E. (2008) *Cell Metab.* **7,** 421–433
18. Whitehead, J. P., Molero, J. C., Clark, S., Martin, S., Meneilly, G., and James, D. E. (2001) *J. Biol. Chem.* **276,** 27816–27824
19. Shewan, A. M., van Dam, E. M., Martin, S., Luen, T. B., Hong, W., Bryant, N. J., and James, D. E. (2003) *Mol. Biol. Cell* **14,** 973–986
20. Ramm, G., Larance, M., Guilhaus, M., and James, D. E. (2006) *J. Biol. Chem.* **281,** 29174–29180
21. Larance, M., Ramm, G., Stöckli, J., van Dam, E. M., Winata, S., Wasinger, V., Simpson, F., Graham, M., Junutula, J. R., Guilhaus, M., and James, D. E. (2005) *J. Biol. Chem.* **280,** 37803–37813
22. Govers, R., Coster, A. C., and James, D. E. (2004) *Mol. Cell. Biol.* **24,** 6456–6466
23. Lopez, J. A., Burchfield, J. G., Blair, D. H., Mele, K., Ng, Y., Vallotton, P., James, D. E., and Hughes, W. E. (2009) *Mol. Biol. Cell* **20,** 3918–3929
24. Sano, H., Kane, S., Sano, E., Mîinea, C. P., Asara, J. M., Lane, W. S., Garner, C. W., and Lienhard, G. E. (2003) *J. Biol. Chem.* **278,** 14599–14602
25. Gross, D. N., van den Heuvel, A. P., and Birnbaum, M. J. (2008) *Oncogene* **27,** 2320–2336
26. Adam, R. M., Mukhopadhyay, N. K., Kim, J., Di Vizio, D., Cinar, B., Boucher, K., Solomon, K. R., and Freeman, M. R. (2007) *Cancer Res.* **67,** 6238–6246
27. Ding, J., and Du, K. (2009) *Mol. Cell. Biol.* **29,** 1459–1471
28. Stöckli, J., Davey, J. R., Hohnen-Behrens, C., Xu, A., James, D. E., and Ramm, G. (2008) *Mol. Endocrinol.* **22,** 2703–2715
29. Standaert, M. L., Galloway, L., Karnam, P., Bandyopadhyay, G., Moscat, J., and Farese, R. V. (1997) *J. Biol. Chem.* **272,** 30075–30082
30. Simons, K., and Ikonen, E. (1997) *Nature* **387,** 569–572
31. Gonzalez, E., and McGraw, T. E. (2009) *Proc. Natl. Acad. Sci. U.S.A.* **106,** 7004–7009
32. Kohn, A. D., Summers, S. A., Birnbaum, M. J., and Roth, R. A. (1996) *J. Biol. Chem.* **271,** 31372–31378
33. Ng, Y., Ramm, G., Lopez, J. A., and James, D. E. (2008) *Cell Metab.* **7,** 348–356
34. Geraghty, K. M., Chen, S., Harthill, J. E., Ibrahim, A. F., Toth, R., Morrice, N. A., Vandermoere, F., Moorhead, G. B., Hardie, D. G., and MacKintosh, C. (2007) *Biochem. J.* **407,** 231–241
35. Saito, T., Jones, C. C., Huang, S., Czech, M. P., and Pilch, P. F. (2007) *J. Biol. Chem.* **282,** 32280–32287
36. Schenck, A., Goto-Silva, L., Collinet, C., Rhinn, M., Giner, A., Habermann, B., Brand, M., and Zerial, M. (2008) *Cell* **133,** 486–497